THE JOURNAL OF PHYSICAL CHEMISTRY B

Article

pubs.acs.org/JPCB

Mechanism and Energetics of Ligand Release in the Aspartate Transporter Glt_{Ph}

Germano Heinzelmann,[†] Turgut Bastug,[‡] and Serdar Kuyucak*[,†]

[†]School of Physics, University of Sydney, NSW 2006, Australia

[‡]Department of Materials Science and Nanotechnology Engineering, TOBB Economy and Technology University, Ankara, Turkey

ABSTRACT: The bacterial aspartate transporter Glt_{Ph} cotransports three Na^+ ions with the substrate. The mechanism and energetics of ligand binding have previously been studied using molecular dynamics simulations on the crystal structure of Glt_{Ph} captured in the outward-facing state. Here we use the recent crystal structure of the inward-facing state of Glt_{Ph} to study the reverse process of unbinding of ligands. Gating behavior is studied in the presence of different ligands. A detailed characterization of the intracellular gate is given, pointing out the differences from the extracellular gate. We then perform free energy simulations to calculate the binding affinities of all the ligands in different combinations, from which the unbinding order is determined as Na2, (gate opens), Asp, Na1, and Na3. The strong coupling between Asp and Na1 is quantified from several free energy calculations. Na3 has the largest affinity to Glt_{Ph}, and therefore, its unbinding is proposed as the rate-limiting step in the transport cycle. The release time of Na3, estimated from Kramers' rate theory, is shown to be consistent with the experimental turnover rate of the transporter.

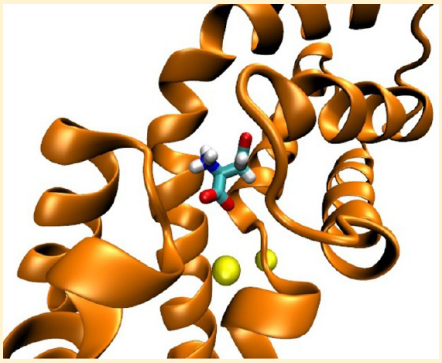

INTRODUCTION

Mammalian glutamate transporters, known as excitatory amino acid transporters (EAATs), are membrane proteins responsible for clearing the excess glutamate released at the nerve synapses. Malfunctioning of glutamate transporters has been implicated in many pathological conditions including cerebral ischemia, amyotrophic lateral sclerosis, and Alzheimer's disease.[1] The transport mechanism of EAATs involves the cotransport of three Na^+ ions and one H^+ ion with the substrate and the countertransport of one K^+ ion.[2,3] Glutamate transporters function by cycling between two states: one facing the extracellular (EC) medium where the ligands bind to the transporter, and the other facing the intracellular (IC) medium where the ligands are released to the cytoplasm. The first crystal structure of an archeal homologue of EAATs—the aspartate transporter Glt_{Ph} from *Pyrococcus horikoshii*—was determined in the outward-facing state.[4] In subsequent crystal structures of this state, Glt_{Ph} was captured both in the open and closed conformations, and the binding sites for the substrate and two ions were identified.[5] Recently, the crystal structure of Glt_{Ph} was reported in the inward-facing closed state, also complexed with the substrate and two ions.[6] So far, there is no crystal structure available for the inward-facing open state of Glt_{Ph}.

Glt_{Ph} shares about 37% sequence identity with the EAATs, but the homology is much larger for the residues involved in the binding of the ligands, with almost all of them being conserved.[7−10] Experiments have shown that, while the transport mechanism in Glt_{Ph} is independent of H^+ and K^+ ions,[11] it is still coupled to the cotransport of three Na^+ ions as in EAATs.[12] The third Na^+ site could not be identified in the crystal structures of Glt_{Ph}, but a binding site determined from molecular dynamics (MD) simulations was confirmed from mutagenesis experiments and shown to be conserved in Glt_{Ph} and the EAAT family.[13] Due to the structural and functional similarities between these proteins, and in the absence of any crystal structures for the EAATs, Glt_{Ph} provides a good model to interpret functional data on EAATs and gain new insights into the transport mechanism.[14,15]

Several MD simulations have been performed on the outward-facing state of Glt_{Ph}, to study the opening of the HP2 segment which works as the EC-gate,[16,17] to find the location of the Na3 site,[13,18,19] and to calculate the binding free energies of the ligands.[19,20] MD simulations and elastic network models have also been used to study substrate translocation[21−24] and release.[25] In an interesting application of metadynamics simulations, Grazioso et al.[26] investigated the mechanism of substrate uptake and release and calculated the free energy surfaces for opening of the EC and IC-gates with different combinations of bound ligands. This study revealed the following: (i) Contrary to the outward-facing state where only the HP2 segment works as the EC-gate, opening of the IC-gate involves the movement of both HP1 and HP2. (ii) There is an energy barrier between the open and closed conformations of the IC-gate, which is not seen in the case of the EC-gate. We note that the metadynamics simulations were carried out using a single monomer in solution instead of a trimer embedded in membrane and in the absence of the Na3 ion. It is important to confirm that the gating results obtained

Received: January 30, 2013
Revised: March 22, 2013
Published: April 16, 2013

in ref 26 are retained in a more realistic environment and in the presence of the Na3 ion.

In a previous paper,[20] we performed detailed free energy simulations in the outward-facing state of Glt_{Ph} with an Asp and three Na^+ ions as ligands. From the binding free energies of ligands in different configurations, we determined their binding order as Na3, Na1, Asp, (EC-gate closes), and Na2. A key finding of this work is that Asp and Na1 are coupled through a hydrogen-bond network despite being separated by about 7 Å. Here we perform a similar study for the inward-facing state of Glt_{Ph}. We first investigate the opening of the IC-gate by performing unbiased MD simulations with different combinations of the bound ligands. This is followed by free energy calculations of the binding affinities for Na2 in the closed configuration, and for other ligands in the open configuration. As in the outward-open case, we find a close link between binding of Asp and Na1; namely, Asp can only bind in the presence of Na1, and it is released to the cytoplasm when Na1 is removed from the binding site. The binding free energy results indicate that the ligands are released in a reverse order compared to their binding, that is, Na2, (IC-gate opens), Asp, Na1, and Na3. The Na3 ion is released last with a binding affinity much higher than the other ligands, which suggests that this step is the rate-limiting step of the transport cycle.

METHODS

Model System and Simulation Details. There are several crystal structures of Glt_{Ph} available from the Protein Data Bank, most of them in the outward-facing state.[4,5] In this study, we use the crystal structure of Glt_{Ph} K55C−A364C mutant cross-linked with divalent mercury, which is in the inward-facing, closed conformation with two Na^+ ions (Na1 and Na2) and Asp bound (PDB ID: 3KBC).[6] We chose this structure here because our goal is to study the mechanism and energetics of release of the ligands to the cytoplasm. As in the other crystal structures of Glt_{Ph}, the Na3 site was not resolved in 3KBC. Therefore, we add a third Na^+ ion at the Na3 site identified in ref 13, where it is coordinated by the side chains of D312, N310, T92, and S93 and the backbone carbonyl of Y89. Justification for this site comes from mutagenesis experiments,[13] which show that the T92A and S93A mutations significantly reduce Na^+ affinity to the transporter. Also, when an alternative Na3 site is used in MD simulations, the D312 side chain swings away from the crystal structure position by about 6 Å and starts coordinating Na1, which is in conflict with the Na1 coordination shell found in the crystal structure.[13]

The simulation system is prepared using the software VMD.[27] We first embed the crystal structure of the Glt_{Ph} trimer in a 1-palmitoyl-2-oleoyl-phosphatidylethanolamine (POPE) phospholipid bilayer containing 251 POPE molecules. Each subunit of Glt_{Ph} has four ligands bound: three Na^+ ions, namely, Na1, Na2, and Na3, and Asp as the substrate. We then solvate the protein−membrane complex in a box of 16204 water molecules with 34 Na^+ ions and 43 Cl^- ions. The extra Cl^- ions are required to keep the simulation box neutral, and their number changes depending on the ligands bound to the transporter. The system is then equilibrated in two stages. In the first stage, the coordinates of the ligands and protein atoms are fixed and the system is equilibrated with 1 atm pressure coupling in all directions until the correct water and lipid densities are obtained. At this point, the x- and y-dimensions of the simulation box are fixed, and pressure coupling is applied only in the z direction thereafter (typical dimensions of the simulation box are $114 \times 112 \times 75$ Å^3). In the second stage, the protein is gradually relaxed by reducing the restraints on the protein atoms in several steps during MD simulation lasting 2.4 ns. The system is then further equilibrated for 10 ns without restraints before we start collecting data.

All of our MD simulations are performed using the NAMD package (version 2.8)[28] with the CHARMM22 force field[29] including the CMAP dihedral corrections.[30] We note that the latest version (CHARMM36) has an updated force field for lipids but not for proteins. We have checked that using CHARMM36 instead of CHARMM22 yields essentially the same results for the binding free energies of ligands. The temperature is maintained at 300 K using Langevin damping with a coefficient of 5 ps^{-1}, and the pressure is kept at 1 atm using the Langevin piston method with a damping coefficient of 20 ps^{-1}.[31] Periodic boundary conditions with the particle-mesh Ewald method are employed to calculate the electrostatic interactions without truncation. The Lennard-Jones (LJ) interactions are switched off between 10 and 12 Å using a smooth switching function. A time step of 2 fs is used in all MD simulations.

Free Energy Calculations. We use essentially the same methods as in our previous work[20] in calculation of the binding free energies of ligands. Therefore, we briefly review the free energy methods here and refer to ref 20 for details. The standard binding free energy of a ligand can be expressed as[32−34]

$$\Delta G_b = \Delta G_{tr} + \Delta G_{rot} + \Delta G_{con} + \Delta G_{int} \quad (1)$$

Here the first two terms give the free energy change due to translational and rotational entropy loss upon binding, the third term measures the free energy cost of applying conformational restraints on the ligand in the binding site relative to bulk, and the last term represents the free energy of translocating the restrained ligand from the bulk to the binding site. The translational and rotational free energy differences are determined using[35−38]

$$\Delta G_{tr} = -k_B T \ln\left[\frac{(2\pi e)^{3/2}\sigma_x\sigma_y\sigma_z}{V_0}\right],$$
$$\Delta G_{rot} = -k_B T \ln\left[\frac{(2\pi e)^{3/2}\sigma_{\phi 1}\sigma_{\phi 2}\sigma_{\phi 3}}{8\pi^2}\right] \quad (2)$$

where V_0 = 1660 Å^3, σ_x, σ_y, and σ_z are the principle rms fluctuations of the center of mass of the ligand in the binding site and $\sigma_{\phi 1}$, $\sigma_{\phi 2}$, and $\sigma_{\phi 3}$ are the rotational rms fluctuations of the ligand calculated using the quaternion representation.[38] The various σ values are estimated from 8 ns of MD simulations of the bound ligands with no restraints applied.

The free energy cost of applying conformational restraints is determined using[39]

$$\Delta G_{con} = \frac{1}{2}\int_0^{k_f} \langle |\mathbf{X} - \mathbf{X}_0|^2 \rangle \, dk \quad (3)$$

where $|\mathbf{X} - \mathbf{X}_0|$ represents the difference of the restrained coordinates from the reference values at a given k. The integral is evaluated using 10 windows with k = 4.0, 2.0, 1.0, 0.5, 0.2, 0.1, 0.05, 0.02, 0.01, and 0 kcal/mol/Å^2. Each window is simulated for 600 ps, and the ensemble average of the coordinate difference is calculated from the last 300 ps. For the bulk simulations, we use a box containing the ligand and 1193

dx.doi.org/10.1021/jp4010423 | J. Phys. Chem. B 2013, 117, 5486−5496

water molecules (plus counterions to keep the system neutral). The value of ΔG_{con} is then obtained from $\Delta G_{con} = \Delta G_{con}^{bulk} - \Delta G_{con}^{site}$.

The free energy of translocation, G_{int}, is calculated using the free energy perturbation (FEP) and thermodynamic integration (TI) methods.[40] In the FEP method, the interval between $\lambda = 0$ and 1 is divided into n subintervals with $\{\lambda_i = 1, ..., n - 1\}$, and for each subinterval, the free energy difference is calculated from the ensemble average

$$\Delta G_i = -k_B T \ln\langle \exp[-(H(\lambda_{i+1}) - H(\lambda_i))/k_B T]\rangle_{\lambda_i} \quad (4)$$

where $H(\lambda) = (1 - \lambda)H_0 - \lambda H_1$, with H_0 and H_1 representing the free-ligand and bound-ligand states. The free energy of translocation is obtained from the sum $\Delta G_{int} = \sum_i \Delta G_i$. For electrostatic interactions, we use exponentially spaced subintervals which are smaller near the end points, with a total of 66 windows.[20] In a typical FEP calculation, each window is equilibrated for 40 ps followed by 40 ps of production. In the TI method, the ensemble average of the derivative, $\partial H(\lambda)/\partial\lambda$, is obtained at several λ values, and the free energy of translocation is calculated from the integral

$$\Delta G_{int} = \int_0^1 \left\langle \frac{\partial H(\lambda)}{\partial \lambda} \right\rangle_\lambda d\lambda \quad (5)$$

Provided the integrand can be fitted well with a polynomial, Gaussian quadrature provides an efficient and accurate method for evaluation of such integrals because it allows for longer sampling of a smaller number of windows. This is the case for all of our calculations; therefore, we use a seven-point quadrature for the TI simulations that involve electrostatic interactions.[41] Seven windows are found to be insufficient for the LJ interactions, so a 9- or 12-point quadrature has been used in this case. All the TI windows are created from the previous FEP runs, which have already been equilibrated. Each window is sampled for 0.8 ns, of which the last 0.7 ns is used for production. Adequacy of this protocol is demonstrated from the running averages of the free energy differences which converge to a flat line, and from lack of hysteresis effects between the forward and backward calculations. In addition, the free energies calculated using the FEP and TI methods agree within statistical fluctuations. To prevent duplication, we report here only the TI results, which are expected to be slightly more accurate due to longer sampling of each window.

For the Na^+ ions, only two of the terms in eq 1 contribute to the binding free energy, ΔG_{tr} and ΔG_{int}. All the Na sites are observed to be occupied by a water molecule in the absence of the ion. Thus, ΔG_{int} is calculated by alchemically transforming a Na^+ ion in one of the binding sites to a water molecule while a water molecule in the bulk is simultaneously transformed to a Na^+ ion. The backward calculation for the reverse process is also performed, and ΔG_{int} is determined from their average as $\Delta G_{int} = (-\Delta G_{int}^{for} + \Delta G_{int}^{back})/2$.

Due to its more complex nature, we adopt a staged approach for free energy calculations of Asp.[34] Accordingly, Asp is restrained in the binding site and the electrostatic and LJ interactions are switched off one at a time, which results in annihilation of Asp in the binding site. A reverse process is performed in the bulk simultaneously, resulting in creation of a restrained Asp in the bulk, which is then unrestrained. The reference positions for the restrained atoms are chosen so that there is a maximal overlap between the restrained and unrestrained Asp. The LJ interactions are switched off using a soft-core LJ potential with a shift coefficient of 5.0.[42] To avoid trapping of water molecules under the substrate during the backward LJ calculation, it is performed in two stages: first, the neutral backbone is created/destroyed, and then, the neutral side chain is created/destroyed. This approach is also used in the forward LJ calculation to preserve symmetry. Thus, the forward free energy of translocation is given by $\Delta G_{int}^{for} = \Delta G_{elect} + \Delta G_{LJ-bb} + \Delta G_{LJ-sc}$), where the three terms represent the contributions from the electrostatic interactions, LJ−backbone, and LJ−side chain. ΔG_{elec} is calculated by discharging Asp in the binding site while an uncharged Asp in the bulk (30 Å away from the binding site) is charged simultaneously. In the second and third stages, the LJ interactions for the side chain and backbone of the uncharged Asp in the binding site are switched off while they are switched on for an uncharged Asp in the bulk (see ref 20 for details).

Kramers' Rate Theory. The binding free energies of ions, especially that of Na3, are quite large, which may delay their release to the bulk considerably. Therefore, it is important to show that the estimated release times are consistent with the observed turnover rates in Glt_{Ph}. For this purpose, we use Kramers' rate theory,[43,44] which provides an estimate for the rate of escape of a particle from a binding pocket over a barrier described by a one-dimensional external potential energy function $U(x)$

$$k = \frac{\omega_a}{2\pi}\left\{\left[1 + \left(\frac{\zeta}{2\omega_b}\right)^2\right]^{1/2} - \frac{\zeta}{2\omega_b}\right\}\exp(-U_b/k_B T) \quad (6)$$

Here U_b is the barrier height, ω_a and ω_b are the frequencies of the harmonic potentials at the bottom of the well and top of the barrier, and ζ is the friction coefficient which is related to the diffusion coefficient via the Einstein relation, $\zeta = k_B T/mD$. We assume an inverse harmonic potential for the barrier with height U_b and range x_b. Because $U(x)$ is an external potential energy, U_b is taken from the enthalpic contribution to the binding free energy of the ion. The frequency, ω_b, can be determined from $U_b = m\omega_b^2 x_b^2/2$. The frequency in the binding pocket follows from the equipartition theorem, $m\omega_a^2\sigma_x^2 = k_B T$, where σ_x is the RMS fluctuation of the particle along the reaction coordinate which is calculated from the MD simulations. We note that, in a low friction environment ($\zeta \ll \omega_b$), the rate coefficient has the maximum value of

$$k_{max} = (\omega_a/2\pi)\exp(-U_b/k_B T) \quad (7)$$

With increasing friction, the rate coefficient steadily decreases, and in the high friction limit ($\zeta \gg \omega_b$), it takes the form $k = k_{max}\omega_b/\zeta$.

RESULTS AND DISCUSSION

Opening of the IC-Gate. In the 3KBC crystal structure of Glt_{Ph}, the IC-gate is closed, and only the Na2 ion has access to the solvent. Thus, using this structure, only the binding free energy of the Na2 ion can be calculated. In order to calculate the binding free energies of the other ligands, we need the open conformation of Glt_{Ph} where the IC-gate is open and the ligands are exposed to the solvent. To find the open conformation, we have performed several 30 ns MD simulations of the 3KBC structure with different ligand configurations. The opening of the IC-gate is monitored using the S277(Cα)−V355(Cα) distance, which has been used

dx.doi.org/10.1021/jp4010423 | J. Phys. Chem. B 2013, 117, 5486−5496

in studies of the opening of the EC-gate previously.[17] The S277 and V355 residues are located at the tips of the HP1 and HP2 hairpins, respectively, and hence provide a good measure for the gate opening. The results of these simulations are summarized below.

(i) All the ligands bound: No perceptible changes are observed in the transporter structure with regard to the opening of the IC-gate. Na2 ion remains bound in all subunits for the entire 30 ns of simulations. Note that the Na2 site is different from the Na2′ site obtained from the crystal structure, which is found to be unstable.[20]

(ii) Asp, Na1, and Na3 bound: Na2 ions are removed from all subunits in the last frame of (i) before running the simulations. In Figure 1A, we show the time evolution of the

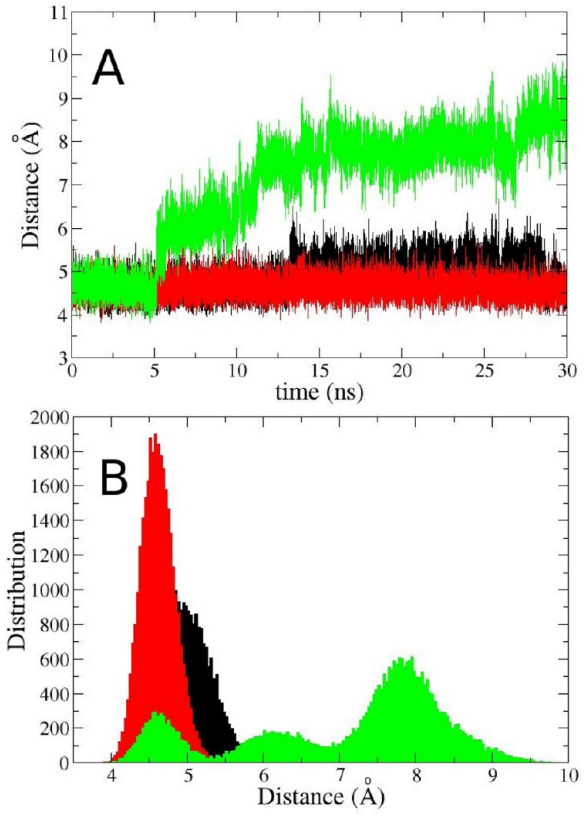

Figure 1. (A) Time evolution of the S277(Cα)−V355(Cα) distance in subunits A (black), B (red), and C (green) when all the ligands are bound except Na2. There is a spontaneous opening of the IC-gate in subunit C starting at 5 ns. (B) The histogram analysis of the same graph, showing the unstable intermediate state in subunit C during the opening of the IC-gate.

S277−V355 distance for the three subunits. The subunits A and B remain in the same state as in (i) and do not show any sign of gate opening. In contrast, subunit C displays a spontaneous opening of the IC-gate at 5 ns with a temporary intermediate state between the open and closed configurations, as can be seen from the histogram of distance distributions (Figure 1B). We note that the EC-gate has not been observed to open in the presence of Asp in MD simulations of the outward structure. The rare event observed in subunit C here is traced to entry of water molecules to the binding pocket through the HP2 segment, which facilitate breaking of the H-bonds that hold the IC-gate. Inspection of the H-bonds during the gate opening shows that the gate is stabilized by two H-bonds HP2 makes with Asp and HP1, namely, Asp(N)−V355(O) and S279(N)−G354(O) (see Table 1). Breaking of the first H-bond results in the half-open intermediate state, and breaking of the second H-bond leads to the fully open state. In the open state, Asp and Na1 are exposed to the solvent, so, in principle, both ligands could unbind at this point.

(iii) Asp and Na3 bound: Simulations are run after removing Na1 ions from all subunits in the last frame of (ii). As shown in Figure 2A, the S277−V355 distances do not show any gating transitions, with subunits A and B remaining in the closed state and C in the open state. Interestingly, Asp in subunit C remains in the binding site for the whole 30 ns, indicating a semistable binding of Asp in the absence of Na1 (see Figure 3A). In contrast, in similar simulations of the outward structure, Asp is released within 5 ns in all subunits. We have, therefore, extended this simulation for a further 20 ns. Asp is eventually observed to lose most of its contacts at 45 ns (Figure 3B).

(iv) Na1 and Na3 bound: Removing Asp instead of Na1 in the last frame of (ii) leads to a very different result. The IC-gates in subunits A and B also open but the gates are extremely unstable, fluctuating freely between the open and closed conformations in all subunits (Figure 2B). This further confirms the role of Asp in stabilizing the IC-gate.

(v) Na3 bound: Removing Na1 from the last frame of (iv) yields very similar results to that observed in (iv) (not shown).

(vi) No ligands: Simulations are run after removing all the ligands from the last frame of (i). All the IC-gates open within 6 ns (Figure 2C). Although the gates still exhibit large fluctuations, they do not visit the fully closed state anymore, indicating that it is less favored in the apo state.

The above results demonstrate that the bound Asp plays an important role in stabilizing the IC-gate via the V355(O)−Asp(N) H-bond. The H-bonds noted in simulation (ii) result in a sizable energy barrier between the open and closed conformations, which suppresses random gating transitions. To confirm the role of these H-bonds in gating and also to create open-states in all subunits, we attempt to break them in simulation (ii) where Asp, Na1, and Na3 are bound. For this purpose, we introduce a repulsive half-harmonic potential defined by $U = 0.5k(r - r_0)^2$ for $r < r_0$ and $U = 0$ for $r < r_0$, with parameters k = 25 kcal/mol/Å^2 and r_0 = 4.5 Å. This potential acts on the H-bond partners only when the distance between the atoms (r) is less than 4.5 Å. It speeds up breaking of the specified H-bonds and thereby facilitates the gate opening process observed in subunit C. Applying this potential to the Asp(N)−V355(O) and S279(N)−G354(O) distances in subunits A and B, we observe that the IC-gate in subunit B quickly opens and remains in this state for almost 10 ns with no bias forces acting as they are outside the range (Figure 4, red line). In subunit A, upon breaking of the S279(N)−G354(O) H-bond, G354(O) forms two intermediate H-bonds with the hydroxyl groups of S277 and S279, keeping the IC-gate closed. These H-bonds are also broken by applying the half-harmonic potentials at 5 ns, after which the IC-gate in subunit A also opens and remains in this state with no bias forces acting (Figure 4, black line). Despite the differences in the opening mechanisms, all three states have very similar final conformations, as demonstrated in the alignment diagram in Figure 5. We stress, in particular, the similarity between the open states obtained using the bias forces (subunits A and B) and the one obtained from MD simulations (subunit C). This is further quantified by calculating the RSMDs between the subunits A−

dx.doi.org/10.1021/jp4010423 | J. Phys. Chem. B 2013, 117, 5486−5496

Table 1. List of the Glt_{Ph} Residues (First Column) and Coordinating Asp Atoms (Second Column)[a]

Glt_{Ph} residue	Asp residue	crystal structure	closed state	open state
HP1−S279 (N)	HP2−G354 (O)	3.3	3.0 ± 0.2	6.0 ± 0.8
HP1−R276 (O)	Asp (αN)	3.1	2.9 ± 0.1	3.0 ± 0.2
HP1−S278 (N)	Asp (α-O_1)	2.5	2.8 ± 0.1	2.9 ± 0.1
HP1−S278 (OH)	Asp (α-O_2)	3.7	2.7 ± 0.1	2.8 ± 0.1
TM7−T314 (OH)	Asp (β-O_2)	2.6	2.7 ± 0.1	2.7 ± 0.1
HP2−V355 (O)	Asp (α-N)	2.1	3.0 ± 0.2	5.5 ± 0.3
HP2−G359 (N)	Asp (β-O_2)	2.7	3.0 ± 0.2	3.2 ± 0.4
TM8−D394 (O_1)	Asp (α-N)	3.4	2.7 ± 0.1	2.7 ± 0.1
TM8−R397 (N_1)	Asp (β-O_2)	3.9	4.3 ± 0.2	2.7 ± 0.1
TM8−R397 (N_2)	Asp (β-O_1)	2.5	2.9 ± 0.2	2.7 ± 0.1
TM8−T398 (OH)	Asp (α-N)	3.6	3.2 ± 0.2	3.0 ± 0.2
TM8−N401 (N_δ)	Asp (α-O_2)	2.9	2.9 ± 0.1	2.9 ± 00.2

[a]The average N−O and O−O distances (in Å) obtained from the MD simulations in the closed and open states are compared to those of the crystal structure 3KBC (third column). Bare O and N atoms in parentheses refer to the backbone atoms, and the others refer to the side chain atoms. The first row shows the S279(N)−G354(O) H-bond distance involved in the IC-gate.

C and B−C after aligning the segments HP1, HP2, TM7, and TM8, which yield 0.9 Å in both cases.

The conformational changes occurring during the opening of the IC-gate are demonstrated in Figure 6A, where the open apo state obtained from the MD simulations is superposed with the closed state obtained from the crystal structure. Opening of the IC-gate involves a partial movement of HP2 toward TM2 and a similarly small movement of HP1 away from HP2; e.g., the S277−V355 distance increases by about 4 Å after the IC-gate opens, while the same distance increases by 10 Å in the EC-gate. As shown in Figure 6B, essentially the same open conformation is obtained from the MD simulations with bound Asp, Na1, and Na3, which is used in the free energy calculations. To show the effect of gate opening on the bound Asp, we present in Table 1 the residues involved in the coordination of Asp, and how the contact distances change when the IC-gate opens. The S279(N)−G354(O) distance is also given in Table 1 because it is involved in the gating. Comparing the results in Table 1 with those obtained for the outward-facing conformation (Table 2 in ref 20), we find a rather different mechanism. Opening of the EC-gate involves breaking of the V355(O)−Asp(N) and G359(N)−Asp(βO_2) bonds, which allows HP2 to move away from a stationary HP1. In opening of the IC-gate, only the first of these HP2−Asp bonds is broken, while the second remains intact and performs a hinge function (Table 1). More importantly, none of the HP1−Asp bonds are broken.

In order to quantify and contrast the changes occurring in the IC and EC-gates further, we show the RMSD of the Cα atoms at the tip of HP1 and HP2 using the closed crystal structures as a reference (Figure 7). Here it is clearly seen that HP2 is the only moving part in the EC-gate, whereas both HP1 and HP2 move in the IC-gate but to a much lesser degree. The movement is also less uniform across the tip with the maximum occurring in the residues S279 in HP1 and A353 in HP2 (indicated in Figure 6B). As noted above, the movement of the HP2 tip is restricted by the unbroken G359−Asp H-bond, which results in partial opening of HP2 around the G359 hinge. We also see that the HP1−Asp bonds are maintained during gating because HP1 moves only a small distance. Thus, the IC-gate involves a smaller opening and preserves the Asp contacts better relative to the EC-gate. As a result, we expect Asp to have a higher affinity on the IC side compared to the EC side, which will affect its release to the cytoplasm. This has already been noted in case (iii) above where Asp is observed to remain in the binding site much longer in the absence of Na1. In order to make sure that the smaller opening of the IC-gate does not prevent the release of Asp, we have facilitated its release by applying repulsive harmonic potentials to the N−O contacts between the R397 side chain and Asp(β-carboxyl) and between the D394 side chain and Asp(α-amino). The same values of potential parameters are employed as in breaking of the H-bonds in the IC-gate. The key events leading to the release of Asp are captured in four snapshots in Figure 8:

Frame A: This is the same snapshot as in Figure 3A (MD simulations with only Asp and Na3 bound after 45 ns). Most of the contacts with the Glt_{Ph} residues have already been lost, and Asp is relatively free to move and rotate within the binding pocket. The half-harmonic potentials are applied at this point, and the system is simulated until Asp is released.

Frame B: In this position, the α-carboxyl group of Asp still makes contacts with S278(N) and S279(N), and the β-carboxyl group of Asp with G357(N). There are no other contacts made by Asp.

Frame C: At this point, the G357(N) contact is lost, and the Asp side-chain moves up toward the solution and away from the binding site. The S278(N) and S279(N) contacts are still maintained.

Frame D: Finally, the S278(N) and S279(N) contacts are also lost, and Asp is released to the cytoplasm.

A similar picture is obtained for the opening of the IC-gate from metadynamics simulations; e.g., the IC-gate remains closed in the presence of Na2, opening of the IC-gate involves movement of both HP1 and HP2, and there is an energy barrier between the open and closed conformations.[26] The metadynamics simulations were performed for a monomer in solution with two bound Na^+ ions. Our results confirm that the basic features of the gating dynamics are not influenced by embedding the Glt_{Ph} trimer in membrane and including the third Na^+ ion. This indicates that Na3 is not involved in gating or coupling to Asp; rather, it provides the electrostatic energy needed to move the binding pocket from the EC to IC side.

Binding Free Energies. The binding free energies of Na^+ ions are calculated using the formalism described in the Methods section, and the results are presented in Table 2. Convergence of the translocation free energies and lack of hysteresis effects are demonstrated in Figure 9. We first discuss binding of Na2, which is bound to the closed state and already

dx.doi.org/10.1021/jp4010423 | J. Phys. Chem. B 2013, 117, 5486−5496

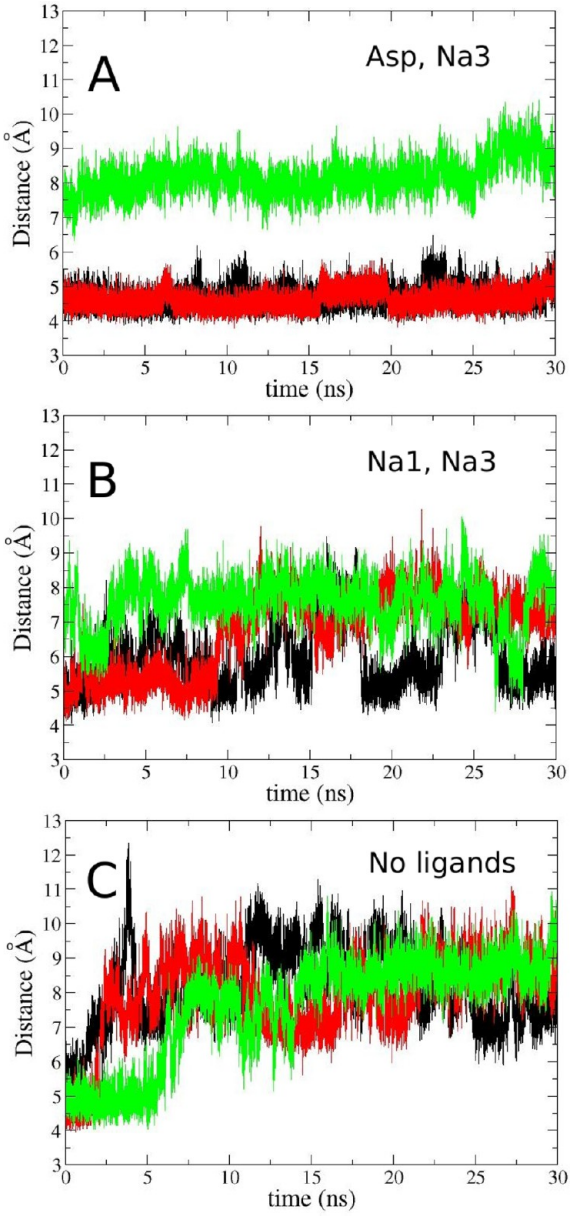

Figure 2. Similar to Figure 1A but for different combinations of bound ligands. (A) Only Asp and Na3 are bound. (B) Only Na1 and Na3 are bound. (C) No ligands are bound. The gate distances are stable in case A but exhibit large fluctuations in B and C. This indicates that the presence of Asp results in an energy barrier between the open and closed conformations.

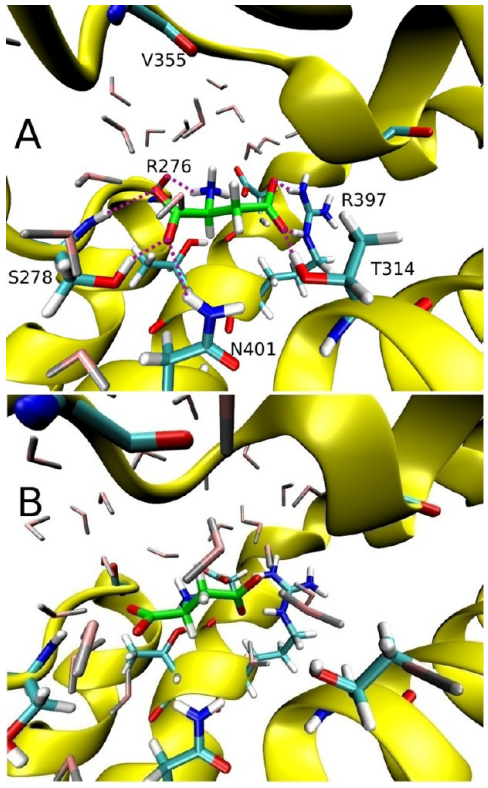

Figure 3. (A) Position of Asp in the binding site in the absence of Na1 after 10 ns of MD simulations. Contacts are indicated with purple dashed lines. (B) The same after 45 ns of simulations, where Asp has lost most of the contacts indicated in part A.

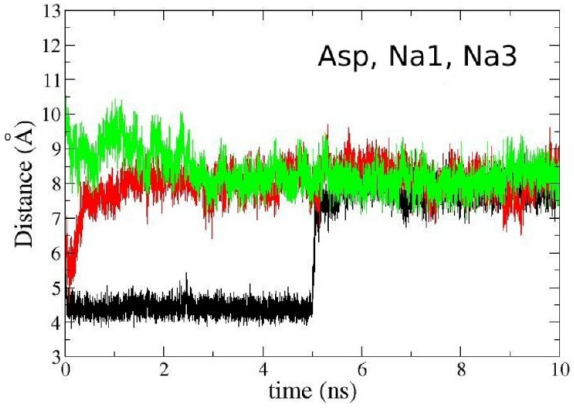

Figure 4. Time evolution of the distance in Figure 1A in a 10 ns simulation with Asp, Na1, and Na3 bound. Here a bias force is introduced into subunits A (black) and B (red) to observe the opening of the IC-gate in these subunits. Even though the bias force does not act after the IC-gate opens, the transporter is seen to remain in the open state, indicating the presence of an energy barrier between the two states when there is a bound Asp.

exposed to the solvent, so it should be the first ligand to be released. The free energy calculation is performed using the closed crystal structure 3KBC. In the outward crystal structure, Na2 is coordinated by the backbone oxygens of T308, S349, I350, and T352. However, in MD simulations, Na2 is observed to shift away from the S349 backbone oxygen immediately, which we call the Na2′ site.[20] With further equilibration, the S349 oxygen is replaced by the side chain oxygen of T308 in all subunits and Na2 remains stably bound in this position.[20] The same thing is observed to happen in the inward structure simulations albeit more slowly, resulting in an identical coordination shell for Na2 as in the inward structure. The calculated Na2 binding free energy is −2.4 kcal/mol, which is also similar to the value obtained for the outward structure, −2.7 kcal/mol.[20] The binding free energy for the Na2′ site is +2.2 kcal/mol, indicating its instability. We note that the Na2 site is not as well located as the Na1 and Na3 sites due to Tl^+ substitution and intrinsic flexibility of the binding site, so there is still some uncertainty about its exact location.

Once the IC-gate is open, the binding pocket is exposed to the solvent, and either Asp or Na1 can unbind. To cover both possibilities, we calculate the Na1 binding free energy in two cases: with only Na3 bound and with Na3 and Asp bound.

dx.doi.org/10.1021/jp4010423 | J. Phys. Chem. B 2013, 117, 5486−5496

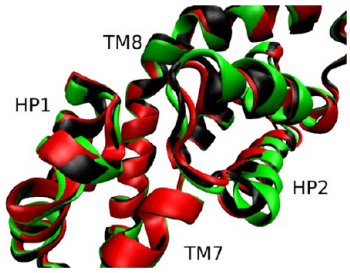

Figure 5. Comparison of the open states obtained using bias forces in subunits A (black) and B (red) with the one obtained from MD simulations in subunit C (green).

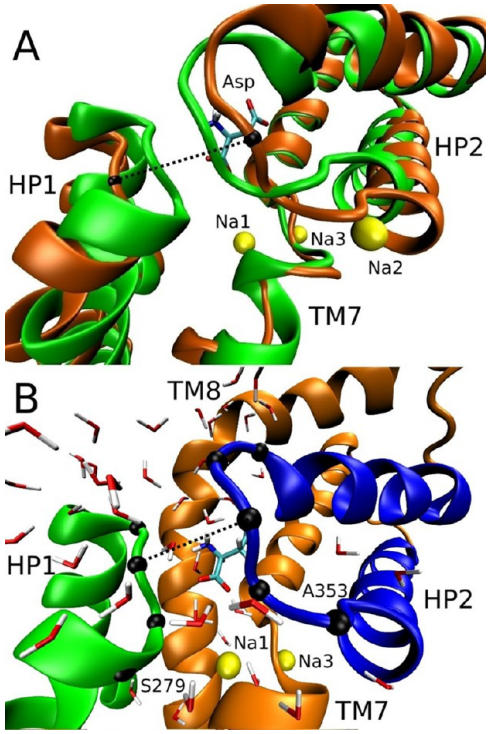

Figure 6. (A) Comparison of the closed state taken from the crystal structure (green) and the open state obtained from the MD simulations with no bound ligands (orange). The black dotted line indicates the S277(Cα)−V355(Cα) distance used in measuring the opening of the IC-gate. (B) The open state obtained from the simulations with Na1, Na3, and Asp bound. In this conformation, both Na1 and Asp have access to the solvent. The Cα atoms used in RMSD measurements in Figure 7 (R276−S279 and A353−G357) are indicated with black spheres.

These and the remaining free energy calculations are performed using the open structure obtained from the MD simulations (subunit C in Figure 1). The Na1 binding free energy in the presence of Na3 is found to be −7.3 kcal/mol, which is very close to the value obtained for the outward structure under the same conditions (−7.1 kcal/mol).[20] This is expected because the same residues coordinate Na1 in the inward and outward structures. From Table 2, the presence of Asp is seen to have a big influence on the binding affinity of Na1, boosting its binding free energy by −7.6 to −14.9 kcal/mol. In the outward structure calculations,[20] we provided a qualitative demonstration of the Asp−Na1 coupling via a hydrogen-bond network, which linked the α-carboxyl group of Asp with Na1. Because Asp(α-carboxyl) and Na1 are separated by 7 Å with a water

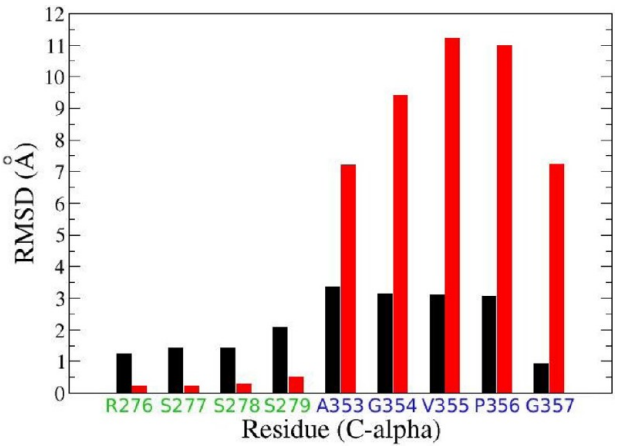

Figure 7. Comparison of the IC-gate opening (black) with the EC-gate opening (red). The RMSDs of the open-state Cα atoms at the tips of HP1 and HP2 are measured with respect to the closed crystal structure after aligning the segments HP1, HP2, TM7, and TM8.

molecule and the S278−OH group in between them (see Figure 10), the strength of this coupling is not clear. In the outward structure, Asp is not stable in the absence of Na1, and therefore, the Na1 binding free energy could not be calculated in the presence of Asp. In the inward structure, Asp remains stable in the absence of Na1 long enough to allow such a calculation. The above estimate of the 7.6 kcal/mol difference in Na1 binding free energies with and without Asp indicates that the Asp−Na1 coupling is fairly strong despite their sizable separation. We emphasize this point because, unlike in LeuT transporters where a Na^+ ion is in direct contact with the substrate,[45] the nature and strength of the substrate−ion coupling is not obvious in Glt_{Ph}.

In order to investigate the nature of the Asp−Na1 coupling and examine the role of the electrostatic interactions between Asp and Na1 in this coupling, we repeat the Na1 binding free energy calculation in the presence of Na3 and Asp but with a neutralized α-carboxyl group. This is expected to abolish the electrostatic interaction between Asp and Na1 because the β-carboxyl and α-amino groups of Asp are at similar distances from Na1 (10 Å) so their effects should mostly cancel each other (Figure 10). The calculated binding free energy (−4.2 kcal/mol) is about 3.1 kcal/mol larger than the value obtained in the absence of Asp (−7.3 kcal/mol). Thus, other factors also contribute to the Asp−Na1 coupling besides the direct electrostatic interactions. For example, the α-carboxyl group of Asp is involved in the H-bond network responsible for binding of Asp,[20] and its neutralization will affect this H-bond network.

Na3 is buried in the protein and can only be released after Na1 and Asp. We calculate the binding free energy of Na3 using the last frame from the 20 ns MD simulations with only Na3 bound. The calculated value (−16.3 kcal/mol) is again comparable to the value obtained for the outward-facing state (−18.7 kcal/mol), reflecting the fact that Na3 coordination is also similar in the inward and outward structures. The Na3 ion has by far the largest affinity of all the ligands, with a high enthalpic barrier (20.7 kcal/mol) that has to be crossed for this ion to be released. We use Kramers' rate theory discussed in the Methods section to provide a rough estimate for the release time of Na3. The barrier potential is specified with height U_b = 20.7 kcal/mol and range $x_b \sim 4$ Å (half of the distance from the

dx.doi.org/10.1021/jp4010423 | J. Phys. Chem. B 2013, 117, 5486−5496

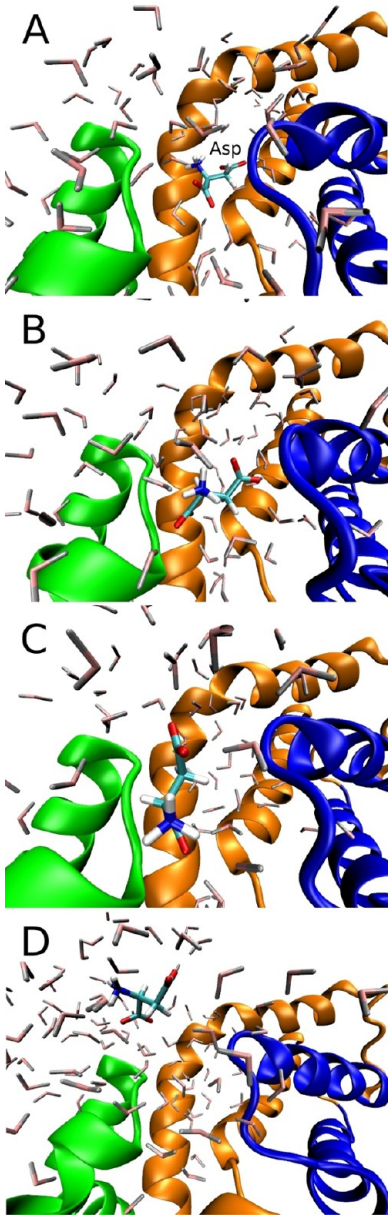

Figure 8. Four snapshots depicting the release of Asp. Explanations are given in the text.

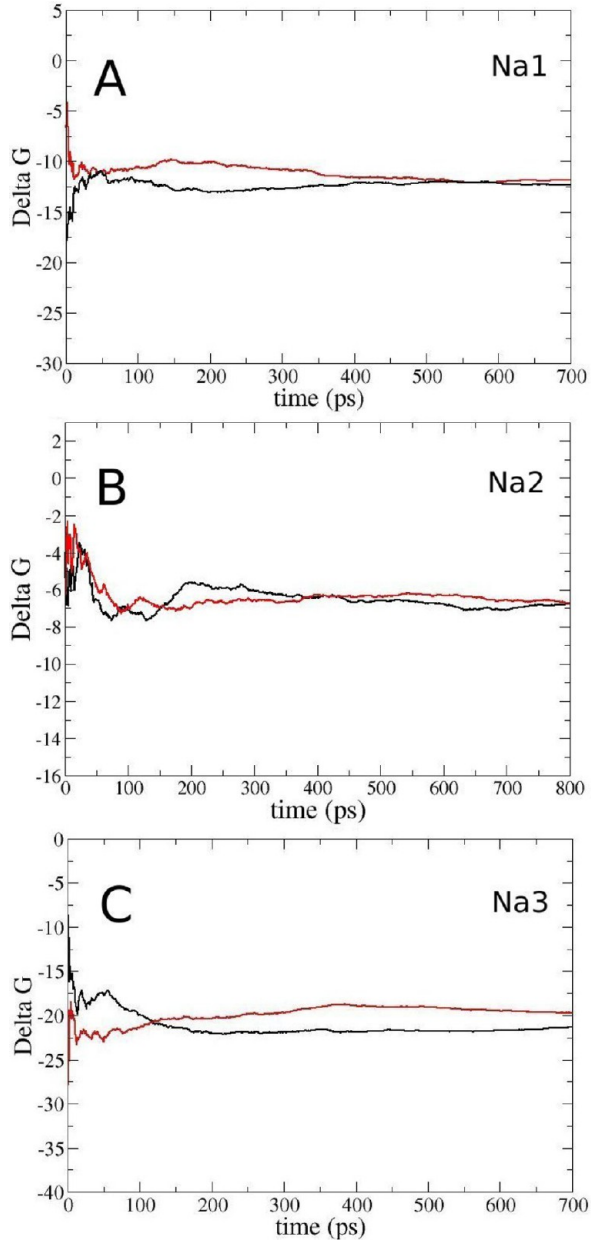

Figure 9. Convergence of the TI results for the translocation free energy of the (A) Na1, (B) Na2, and (C) Na3 ions from running averages. For the Na1 ion, we show the case with only Na3 bound, and the Na2 calculation is for the closed state with all the ligands present. The negative of the forward (binding site → bulk) and backward transitions of Na^+ is shown with black and red lines, respectively.

Na3 site to solvent which is 8 Å), from which we obtain $\omega_b = 7 \times 10^{12}$ s^{-1}. Similarly, from the RMSD fluctuations of the Na3 ion in the binding pocket ($\sigma_x = 0.2$ Å), we obtain $\omega_a = 16 \times 10^{12}$ s^{-1}. From eq 7, these values correspond to a maximum rate

Table 2. Binding Free Energies for Na^+ Ions in the Closed state (for Na2 and Na2′) and in the Open State (for Na1 and Na3) of Glt_{Ph}[a]

ion	$-\Delta G_{int}^{for}$	ΔG_{int}^{back}	ΔG_{int}	ΔG_{tr}	ΔG_b
Na2 (1, 3, Asp)	−6.8 ± 1.2	−6.7 ± 1.1	−6.8 ± 1.2	4.4	−2.4 ± 1.2
Na2′ (1, 3, Asp)	−2.1 ± 0.8	−2.1 ± 1.0	−2.1 ± 0.9	4.3	+2.2 ± 0.9
Na1 (3, Asp)	−19.3 ± 1.2	−20.0 ± 1.3	−19.6 ± 1.3	4.7	−14.9 ± 1.3
Na1 (3)	−12.3 ± 1.6	−11.8 ± 1.8	−12.1 ± 1.3	4.8	−7.3 ± 1.3
Na3	−21.5 ± 1.5	−19.9 ± 1.2	−20.7 ± 1.1	4.4	−16.3 ± 1.1

[a]The forward and backward calculations of the interaction energy are listed in the second and third columns, and their average, in the fourth column. The total binding free energy that includes the translational free energy difference (fifth column) is given in the last column. Other ligands present in the transporter are indicated in parentheses. Errors are estimated from block data analysis using 100 ps windows. All energies are in kcal/mol.

dx.doi.org/10.1021/jp4010423 | J. Phys. Chem. B 2013, 117, 5486−5496

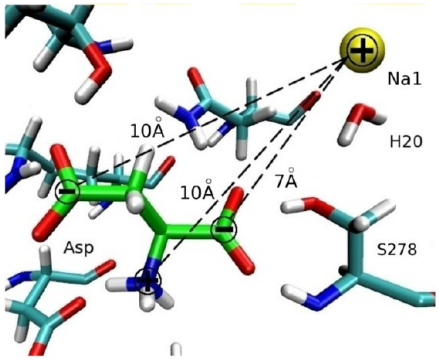

Figure 10. Picture depicting the strong coupling between Asp and Na1. The distances between the charges on Asp and Na1 are indicated with dashed lines. Asp α-carboxyl is closer to Na1 which is the source of strong coupling, while the other positive and negative charges on Asp are at equal distance to Na1 and hence cancel each other.

of $k_{max} = 2.9 \times 10^{-3}$ s^{-1} at $T = 30$ °C, or average release time of 6 min. Including friction in the rate equation (eq 6) will lower the rate and increase the release time. The friction coefficient of Na^+ ions in bulk water is $\zeta = 8 \times 10^{13}$ s^{-1}, which is larger than ω_b. However, there are no water molecules in the Na3 binding pocket, and hence, we expect ζ to be much smaller than the bulk value. As an example, for $\zeta \sim \omega_b$, the rate would be $k = 0.6k_{max} = 1.7 \times 10^{-3}$ s^{-1}, corresponding to an average release time of 10 min.

The experimental turnover time of Glt_{Ph} is 3.5 min at $T = 30$ °C.[11] There is strong support from mutagenesis experiments that unbinding of Na3 is the rate-limiting step in the transport cycle. Mutation of the residues coordinating Na3, which reduce its binding affinity and facilitate its release, result in almost 20-fold increase in the transport rate.[13] Experiments also indicate that the outward−inward transition is relatively rapid (seconds) and does not limit the rate of transport.[6] Thus, assuming that the rate-limiting step in the transport cycle is the release of Na3, the calculated release time is consistent with the experimental turnover time (note that the computational accuracy of free energies is about 1 kcal/mol which translates to a factor of 5 in the rate coefficients or release times).

While the release time of the Na^+ ions is quite long, their electrostatic potential energy provides sufficient incentive for keeping the transporter in the inward conformation until they are released. For a membrane potential of −80 mV, transport of each Na^+ ion against this potential gradient costs 80/25 = 3.2 kT. For two Na^+ ions, the cost is 6.4 kT. Thus, compared to the apo state, transition of the Na1−Na3 bound transporter to the outward-facing state is suppressed by a factor of $\exp(-6.4) \sim 1/600$.

The temperature dependence of Asp uptake provides another test for the proposed model. The Q_{10} value estimated from the Na3 release rates at $T = 25$ and 35 °C is 3.1, which is in reasonable agreement with the measured Q_{10} value of 3.7.[11]

We next consider the binding free energy of Asp in the presence of Na1 and Na3, which is calculated using the open subunit from the last frame of the MD simulations in Figure 1A (Table 3). Convergence of the Asp translocation free energies for various contributions and lack of hysteresis effects are demonstrated in Figure 11. The calculated value (−4.9 kcal/

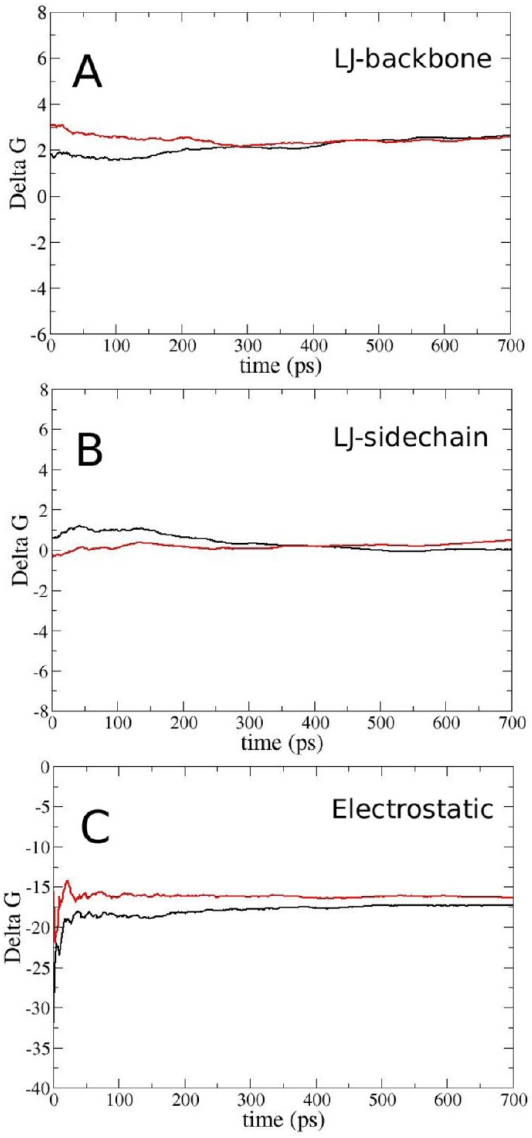

Figure 11. Convergence of the TI results for the three different components of the translocation free energy of aspartate from running averages: (A) the creation/destruction of the neutral backbone, (B) the same for the side-chain, and (C) the charging/discharging of the whole aspartate molecule. Here we show the case in which we have both Na1 and Na3 bound to the transporter. The negative of the forward (binding site → bulk) and backward transitions of Na^+ is shown with black and red lines, respectively.

Table 3. Various Terms Contributing to the Binding Free Energy of Asp in the Open State of Glt_{Ph}[a]

substrate	ΔG_{elec}	ΔG_{LJ-bb}	ΔG_{LJ-sc}	ΔG_{tr}	ΔG_{rot}	ΔG_{con}	ΔG_b
Asp (1,3)	−17.0 ± 1.0	2.6 ± 0.6	0.3 ± 0.6	3.9	4.6	0.7	−4.9 ± 1.1
Asp (3)	−9.3 ± 1.2	1.8 ± 0.7	0.4 ± 0.5	3.9	4.4	0.6	+1.8 ± 1.3

[a]The forward and backward calculations differed by less than 1 kcal/mol in all cases; therefore, only their average is listed. Other ligands present in the transporter are indicated in parentheses. The absolute binding free energy of Asp is given in the last column. Errors are estimated from block data analysis using 100 ps windows. All energies are in kcal/mol.

dx.doi.org/10.1021/jp4010423 | J. Phys. Chem. B 2013, 117, 5486−5496

mol) is 10 kcal/mol higher than the binding free energy of Na1 in the presence of Asp and Na3 (−14.9 kcal/mol), which assures that Na1 is released only after Asp. Thus, the ligands are released into the cytoplasm in the order of Na2, Asp, Na1, and Na3, which is the reverse of their binding order in the outward-facing state.[20] As noted in the discussion of the IC-gate, Asp is better coordinated in the inward structure compared to the outward structure, and this is corroborated by its binding free energy which is 1.1 kcal/mol lower in the inward state relative to the outward state. In fact, the enthalpic contribution to the binding free energy is 2.6 kcal/mol lower in the inward state, but this is partly offset by the entropic contributions which are also higher. All of these point to a tighter binding of Asp in the inward state.

As pointed out above, Asp remains stable in the absence of Na1 long enough (>30 ns) to allow free energy calculations. This means that we can also calculate the binding free energy of Asp in the presence of only Na3 (Table 3). The calculation is performed using the open subunit of the MD simulations in Figure 2A. The calculated value is 1.8 kcal/mol, showing that Asp is indeed unstable in this configuration, but the relatively large enthalpic contribution to the binding free energy (−7.1 kcal/mol) delays its release. Comparing the Asp binding free energies with and without Na1 (Table 3) gives another estimate for the Asp−Na1 coupling. The binding free energy difference is 6.7 kcal/mol, which is consistent with the value obtained from the Na1 binding free energies with and without Asp (7.6 kcal/mol).

CONCLUSIONS

We have performed MD simulations and free energy calculations in the inward-facing state of the Asp transporter Glt_{Ph}. The gating mechanism is studied in equilibrium simulations with different ligands bound to the transporter. Spontaneous opening of the IC-gate with Na1, Na3 ,and Asp bound is observed in one of the MD simulations, which happens through the breaking of two hydrogen bonds. The IC-gate is found to be quite different from the EC-gate, as it involves movement of both HP1 and HP2 but in much smaller amounts. Our results indicate that the presence of Asp leads to an energy barrier between the open and closed states, consistent with the metadynamics simulations.[26] This mechanism presumably facilitates the unbinding of Asp by keeping the transporter in an open state until it is released.

The unbinding order predicted from the binding free energies is Na2, (IC-gate opens), Asp, Na1, and Na3, which is the reverse of the order of binding found in the outward structure.[20] Another difference between the inward and outward structure calculations is the semistable binding of Asp in the inward case when only Na3 is present. This has allowed us to give a quantitative estimate for the strength of the coupling between Asp and Na1, which was only qualitatively described in the previous work.[20] The binding free energy of Na3 is found to be substantially lower than the other ligands, suggesting that its unbinding is the rate-limiting step in the transport process. Estimates of the release time obtained from Kramers' rate theory are consistent with the experimental turnover rate of Glt_{Ph}, which provides further support for this proposal.

The free energy calculations show that the binding free energies of Na^+ ions and Asp in the inward structure are very similar to those obtained from the outward structure. This is expected from the similarity of the binding sites in the inward and outward open state structures. The faster turnover rates observed in mammalian glutamate transporters could result from the extra proton transported and/or changes in the binding sites during the transition, which could facilitate the release of ligands. It will be interesting to see if the homology models of mammalian glutamate transporters could provide such mechanistic explanations for the differences observed between them and Glt_{Ph}.

AUTHOR INFORMATION

Corresponding Author

*E-mail: serdar@physics.usyd.edu.au. Phone: ++61 2-9036-5306.

Notes

The authors declare no competing financial interest.

ACKNOWLEDGMENTS

This work was supported by grants from the Australian Research Council and Turkish Scientific and Technical Research Council. Calculations were performed using the HPC facilities at the National Computational Infrastructure (Canberra) and ULAKBIM (Ankara). We thank Rob Vandenberg and Renae Ryan for discussions on the structure and function of Glt_{Ph}.

REFERENCES

(1) Danbolt, N. C. Glutamate Uptake. *Prog. Neurobiol.* **2001**, *65*, 1−105.

(2) Kanner, B. I.; Bendahan, A. Binding Order of Substrates to the Sodium and Potassium-Ion Coupled L-Glutamic Acid Transporter from Rat-Brain. *Biochemistry* **1982**, *21*, 6327−6330.

(3) Zerangue, N.; Kavanaugh, M. P. Flux Coupling in a Neuronal Glutamate Transporter. *Nature* **1996**, *383*, 634−637.

(4) Yernool, D.; Boudker, O.; Jin, Y.; Gouaux, E. Structure of a Glutamate Transporter Homologue from Pyrococcus Horikoshii. *Nature* **2004**, *431*, 811−818.

(5) Boudker, O.; Ryan, R. M.; Yernool, D.; Shimamoto, K.; Gouaux, E. Coupling Substrate and Ion Binding to Extracellular Gate of a Sodium-Dependent Aspartate Transporter. *Nature* **2007**, *445*, 387−393.

(6) Reyes, N.; Ginter, C.; Boudker, O. Transport Mechanism of a Bacterial Homologue of Glutamate Transporters. *Nature* **2009**, *462*, 880−885.

(7) Vandenberg, R. J.; Arriza, J. L.; Amara, S. G.; Kavanaugh, M. P. Constitutive Ion Fluxes and Substrate Binding Domains of Human Glutamate Transporters. *J. Biol. Chem.* **1995**, *270*, 17668−17671.

(8) Kavanaugh, M. P.; Bendahan, A.; Zerangue, N.; Zhang, Y.; Kanner, B. I. Mutation of an Amino Acid Residue Influencing Potassium Coupling in the Glutamate Transporter GLT-1 Induces Obligate Exchange. *J. Biol. Chem.* **1997**, *272*, 1703−1708.

(9) Bendahan, A.; Armon, A.; Madani, N.; Kavanaugh, M. P.; Kanner, B. I. Arginine 447 Plays a Pivotal Role in Substrate Interactions in a Neuronal Glutamate Transporter. *J. Biol. Chem.* **2000**, *275*, 37436−37442.

(10) Seal, R. P.; Leighton, B. H.; Amara, S. G. A Model for the Topology of Excitatory Amino Acid Transporters Determined by the Extracellular Accessibility of Substituted Cysteines. *Neuron* **2000**, *25*, 695−706.

(11) Ryan, R. M.; Compton, E. L.; Mindell, J. A. Functional Characterization of a Na^+-Dependent Aspartate Transporter from Pyrococcus Horikoshii. *J. Biol. Chem.* **2009**, *284*, 17540−17548.

(12) Groeneveld, M.; Slotboom, D. J. Na^+: Aspartate Coupling Stoichiometry in the Glutamate Transporter Homologue Glt_{Ph}. *Biochemistry* **2010**, *49*, 3511−3513.

(13) Bastug, T.; Heinzelmann, G.; Kuyucak, S.; Salim, M.; Vandenberg, R. J.; Ryan, R. M. Position of the Third Na Site in the

Aspartate Transporter Glt_{Ph} and the Human Glutamate Transporter EAAT1. *PLoS One* **2012**, *7*, e33058.
(14) Jiang, J.; Amara, S. G. New Views of Glutamate Transporter Structure and Function: Advances and Challenges. *Neuropharmacology* **2011**, *60*, 172−181.
(15) Forrest, L. R.; Krämer, R.; Ziegler, C. The Structural Basis of Secondary Active Transport Mechanisms. *Biochim. Biophys. Acta* **2011**, *1807*, 167−188.
(16) Shrivastava, I. H.; Jiang, J.; Amara, S. G.; Bahar, I. Time-Resolved Mechanism of Extracellular Gate Opening and Substrate Binding in a Glutamate Transporter. *J. Biol. Chem.* **2008**, *283*, 28680−28690.
(17) Huang, Z.; Tajkhorshid, E. Dynamics of the Extracellular Gate and Ion-Substrate Coupling in the Glutamate Transporter. *Biophys. J.* **2008**, *95*, 2292−2300.
(18) Huang, Z.; Tajkhorshid, E. Identification of the Third Na^+ Site and the Sequence of Extracellular Binding Events in the Glutamate Transporter. *Biophys. J.* **2010**, *99*, 1416−1425.
(19) Larsson, H. P.; Wang, X. Y.; Lev, B.; Baconguis, I.; Caplan, D. A.; Vyleta, N. P.; Koch, H. P.; Diez-Sampedro, A.; Noskov, S. Y. Evidence for a Third Sodium-Binding Site in Glutamate Transporters Suggests an Ion/Substrate Coupling Model. *Proc. Natl. Acad. Sci. U.S.A.* **2010**, *107*, 13912−13917.
(20) Heinzelmann, G.; Bastug, T.; Kuyucak, S. Free Energy Simulations of Ligand Binding to the Aspartate Transporter Glt_{Ph}. *Biophys. J.* **2011**, *101*, 2380−2388.
(21) Crisman, T. J.; Qu, S.; Kanner, B. I.; Forrest, L. R. Inward-Facing Conformation of Glutamate Transporters as Revealed by Their Inverted-Topology Structural Repeats. *Proc. Natl. Acad. Sci. U.S.A.* **2009**, *106*, 20752−20757.
(22) Gu, Y.; Shrivastava, I. H.; Amara, S. G.; Bahar, I. Molecular Simulations Elucidate the Substrate Translocation Pathway in a Glutamate Transporter. *Proc. Natl. Acad. Sci. U.S.A.* **2009**, *106*, 2589−2594.
(23) Jiang, J.; Shrivastava, I. H.; Watts, S. D.; Bahar, I.; Amara, S. G. Large Collective Motions Regulate the Functional Properties of Glutamate Transporter Trimers. *Proc. Natl. Acad. Sci. U.S.A.* **2011**, *108*, 15141−15146.
(24) Stolzenberg, S.; Khelashvili, G.; Weinstein, H. Structural Intermediates in a Model of the Substrate Translocation Path of the Bacterial Glutamate Transporter Glt_{Ph}. *J. Phys. Chem. B* **2012**, *116*, 5372−5383.
(25) DeChancie, J.; Shrivastava, I. H.; Bahar, I. The Mechanism of Substrate Release by the Aspartate Transporter Glt_{Ph}: Insights from Simulations. *Mol. BioSyst.* **2011**, *7*, 832−842.
(26) Grazioso, G.; Limongelli, V.; Branduardi, D.; Novellino, E.; De Micheli, C.; Cavalli, A.; Parrinello, M. Investigating the Mechanism of Substrate Uptake and Release in the Glutamate Transporter Homologue Glt_{Ph} Through Metadynamics Simulations. *J. Am. Chem. Soc.* **2012**, *134*, 453−463.
(27) Humphrey, W.; Dalke, A.; Schulten, K. VMD - Visual Molecular Dynamics. *J. Mol. Graphics* **1996**, *14*, 33−38.
(28) Phillips, J. C.; Braun, R.; Wang, W.; Gumbart, J.; Tajkhorshid, E.; Villa, E.; Chipot, C.; Skeel, R. D.; Kale, L.; Schulten, K. Scalable Molecular Dynamics with NAMD. *J. Comput. Chem.* **2005**, *26*, 1781−1802.
(29) MacKerell, A. D., Jr.; Bashford, D.; Bellott, M.; Dunbrack, R. L., Jr.; Evanseck, J. D.; Field, M. J.; Fisher, S.; Gao, J.; Guo, H.; Ha, S.; et al. All-Atom Empirical Potential for Molecular Modeling and Dynamics Studies of Proteins. *J. Phys. Chem. B* **1998**, *102*, 3586−3616.
(30) MacKerell, A. D.; Feig, M.; Brooks, C. L. Extending the Treatment of Backbone Energetics in Protein Force Fields. *J. Comput. Chem.* **2004**, *25*, 1400−1415.
(31) Feller, S.; Zhang, Y.; Pastor, R.; Brooks, B. Constant Pressure Molecular Dynamics: the Langevin Piston Method. *J. Chem. Phys.* **1995**, *103*, 4613−4621.
(32) Gilson, M. K.; Given, J. A.; Bush, B. L.; McCammon, J. A. The Statistical-Thermodynamic Basis for Computation of Binding Affinities: A Critical Review. *Biophys. J.* **1997**, *72*, 1047−1069.
(33) Boresch, S.; Tettinger, F.; Leitgeb, M.; Karplus, M. Absolute Binding Free Energies: A Quantitative Approach for Their Calculation. *J. Phys. Chem. B* **2003**, *107*, 9535−9551.
(34) Deng, Y.; Roux, B. Calculation of Standard Binding Free Energies: Aromatic Molecules in T4 Lysozyme L99A Mutant. *J. Chem. Theory Comput.* **2006**, *2*, 1255−1273.
(35) Karplus, M.; Kushick, J. N. Methods for Estimating the Configuratonal Entropy of Macromolecules. *Macromolecules* **1981**, *14*, 325−332.
(36) Luo, H.; Sharp, K. On the Calculation of Absolute Macromolecular Binding Energies. *Proc. Natl. Acad. Sci. U.S.A.* **2002**, *99*, 10399−10404.
(37) Carlson, J.; Aqvist, J. Absolute and Relative Entropies from Computer Simulation with Applications to Ligand Binding. *J. Phys. Chem. B* **2005**, *109*, 6448−6456.
(38) Minh, D. D. L.; Bui, J. M.; Chang, C.; Jain, T.; Swanson, J. M. J.; McCammon, J. A. The Entropic Cost of Protein-Protein Association. *Biophys. J.* **2005**, *89*, L25−L27.
(39) Cecchini, M.; Krivov, S. V.; Spichty, M.; Karplus, M. Calculation of Free-Energy Differences by Confinement Simulations. Application to Peptide Conformers. *J. Phys. Chem. B* **2009**, *113*, 9728−9740.
(40) Beveridge, D. L.; DiCapua, F. M. Free Energy via Molecular Simulation: Applications to Chemical and Biomolecular Systems. *Annu. Rev. Biophys. Biophys. Chem.* **1989**, *18*, 431−492.
(41) Bastug, T.; Kuyucak, S. Energetics of Ion Permeation, Rejection, Binding and Block in Gramicidin A from Free Energy Simulations. *Biophys. J.* **2006**, *90*, 3941−3950.
(42) Zacharias, M.; Straatsma, T. P.; McCammon, J. A. Separation-Shifted Scaling, a New Scaling Method for Lennard-Jones Interactions in Thermodynamic Integration. *J. Chem. Phys.* **1994**, *100*, 9025−9031.
(43) Kramers, H. A. Brownian Motion in a Field of Force and the Diffusion Model of Chemical Reactions. *Physica* **1940**, *7*, 284−304.
(44) Berry, R. S.; Rice, S. A.; Ross, J. *Physical Chemistry*; Oxford University Press: Oxford, U.K., 2000.
(45) Yamashita, A.; Singh, S. K.; Kawate, T.; Jin, Y.; Gouaux, E. Crystal Structure of LEUTAA, a Bacterial Homolog of Na^+/Cl^- Dependent Neurotransmitter Transporters. *Nature* **2005**, *437*, 215−223.